Received: 9 August 2024 | Revised: 19 November 2024 | Accepted: 30 November 2024

DOI: 10.1111/phen.12476

ORIGINAL ARTICLE

Physiological Entomology: How Insects Work - Linking Genotype to Phenotype

Royal Entomological Society

Mechanical properties and cuticle organisation in mandibles are related to the task specialisation in leafcutter ants (*Atta laevigata*, Attini, Formicidae)

Wencke Krings[1,2,3,4] | **Valentin Birkenfeld**[4] | **Stanislav N. Gorb**[4]

[1]Department of Cariology, Endodontology and Periodontology, University of Leipzig, Leipzig, Germany

[2]Department of Electron Microscopy, Institute of Cell and Systems Biology of Animals, University of Hamburg, Hamburg, Germany

[3]Department of Mammalogy and Palaeoanthropology, Leibniz Institute for the Analysis of Biodiversity Change, Hamburg, Germany

[4]Department of Functional Morphology and Biomechanics, Kiel University, Kiel, Germany

Correspondence
Wencke Krings, Department of Cariology, Endodontology and Periodontology, University of Leipzig, Liebigstraße 12, Leipzig 04103, Germany.
Email: wencke.krings@uni-hamburg.de

Associate Editor: Tim Lüddecke

Abstract

Leafcutter ants show a high degree of task division among the workers of different castes. For example, the smallest workers, the minims, care for the brood and the symbiotic fungus, whereas the larger mediae cut and transport plant material. This is reflected in the size and morphology of the mandibles, but also in their mechanical properties as mediae possess the hardest and stiffest cuticle and the minims—the softest and most flexible one. This is directly related to the content of the cross-linking transition metal zinc (Zn). The cuticle microstructure, which can be more or less anisotropic depending on the orientation of cuticle layers, is known to determine the resistance to loads and stresses and thus contributes to the biomechanical behaviour of the structure. To study how the mandible tasks are related to the cuticular organisation, we here documented the microstructure of the mandibles from the mediae and the minims by scanning electron microscopy. Afterwards, the mechanical properties (Youngs' modulus, *E*, and hardness, *H*) of the exo-, meso- and endocuticle were identified by nanoindentation. Tests were performed along the longitudinal and the circumferential axes of the mandibles. We found, that the minims possess mandibles, which are more isotropic, whereas the mandibles of the mediae are rather anisotropic. This difference was never determined within one species before and is probably linked to the task of the individual ant. To gain insight into the origins of these properties, we characterized the elemental composition of the different cuticle layers along the circumferential axis, revealing that only the exocuticle of the mandible cutting edge contains Zn. All other mechanical property gradients thus must be the result of the chitin fibre bundle architecture or the properties of the protein matrix, which awaits further investigation.

KEYWORDS
biomechanics, cuticle, elemental composition, hardness, Hymenoptera, mouthparts, nanoindentation, Young's modulus

INTRODUCTION

Among colony-forming species, leafcutter ants (species of genera *Atta* and *Acromyrmex*) are interesting, as they show a high degree of labour division among the workers of different castes. They can form colonies with millions of individuals with pronounced polyethism and polymorphism based on their symbiosis with fungus, which is farmed on fresh plant material (Cahan & Fewell, 2004; Cherrett, 2019; Leal & Oliveira, 2000).

Atta colonies contain polymorph workers, which are either addressed as minims, minors, mediae, or majors based on their morphologies, tasks and sizes (Arganda et al., 2020; Cahan & Fewell, 2004; Oster & Wilson, 1978; Wetterer, 1999; Wilson, 1983). After the foundation of the colony, workers (head width of 0.8–1.6 mm) performing multiple tasks are produced first. With an increasing number of individuals, the smaller workers (head width of 0.8–1.0 mm) take care of the fungal gardening and the larger ones (head width of 1.6 mm) cut tough plant material. During colony formation, the size spectrum extends (head width of 0.7 to 5 mm), which broadens the plant material used (Püffel, Roces, & Labonte, 2023). Very large individuals, the majors or soldiers, defend the colony against predators; this cast, however, only develops, if the colony possesses millions of individuals as the emergence of the castes depends on colony size (Cahan & Fewell, 2004). Larger individuals (mediae) cut large and thick plant material and carry it into the nest, where it is shredded into smaller pieces, mixed with faeces and shaped into small droplets by smaller workers (minors) (Wirth et al., 2002). Then, even smaller workers use this mass to farm the fungal hyphae, which are then harvested by the smallest and most common workers (minims).

This task division depends on the age of the individuals, as callows (immature ants) care for the nest whereas older ants rather perform tasks outside the nest. This role shift during ontogeny is accompanied by a shift of the biting apparatus (head capsule and muscles), which generates higher forces with increasing individual age (Püffel, Meyer, et al., 2023). However, the task allocation also depends on the polymorphism of the adult workers (Whitehouse & Jaffe, 1996; Wilson, 1980, 1983). As in other ants, these tasks are performed with the mandibles, which show morphological adaptations to their respective roles (Barlow et al., 2019; Birkenfeld et al., 2024; Chowdhury & Rastogi, 2021; Klunk et al., 2021; Klunk, Argenta, Casadei-Ferreira, et al., 2023; Klunk, Argenta, Rosumek, et al., 2023; Püffel et al., 2021; Püffel, Meyer, et al., 2023; Püffel, Roces, & Labonte, 2023; Qi et al., 2023; Richter et al., 2020), and are thus important for the success of the colony (Wilson, 1987; for a review of the feeding apparatus in ants see Richter & Economo, 2023).

Adaptations are, however, reflected not only by the morphology but also by the mechanical properties (e.g. hardness *H* and Young's modulus *E*) of the structures. Cuticle mechanical properties range from KPa to GPa and depend on the composition of the respective region and the water content (Klocke & Schmitz, 2011; Li, Gorb, et al., 2022; see reviews by Vincent & Wegst, 2004; Stamm et al., 2021). Structures, which are prone to abrasions such as mouthparts, joints or claws, are usually significantly harder and stiffer (see, e.g. Schofield et al., 2002, 2021; Barbakadze et al., 2006; Cribb et al., 2008a; Zhang et al., 2019; Tadayon et al., 2020; Kundanati et al., 2020, 2021; Krings & Gorb, 2023) than structures which have a reduced risk of being worn such as legs, eyes, elytra or wings (e.g. Chen et al., 2013; Dirks & Taylor, 2012; Hayot et al., 2013; Li et al., 2020; Li, Rajabi, et al., 2022; Lomakin et al., 2011; Oh et al., 2017; Smith et al., 2000).

With regard to *Atta laevigata* (Smith, 1858), it was previously found that the larger ants (mediae) possess harder and stiffer mandibular exocuticles, followed by the minors, and finally the minims with the softest and most flexible ones (Birkenfeld et al., 2024). This can be explained by the tasks performed by the individuals, as with an increase in the ant and mandible size, the forces increase as well (Püffel, Johnston, et al., 2023; Wilson, 1980, 1983). In other ant taxa, an increase in stress related to ant size was determined (Klunk et al., 2021; Klunk, Argenta, Casadei-Ferreira, et al., 2023; Klunk, Argenta, Rosumek, et al., 2023). In *Atta*, the relationship between size and stress has been previously suggested on the basis of muscular and structural parameters (Püffel et al., 2021) and tested in bite-force experiments (Püffel, Meyer, et al., 2023; Püffel, Roces, et al., 2023). The higher mechanical property values of the mandibular exocuticle of the *A. laevigata* mediae are likely an adaptation to reduce the risk of structural failure when experiencing higher stresses, and wear, when cutting challenging plant materials (Birkenfeld et al., 2024).

Arthropod cuticle is a multifunctional composite material (see Vincent & Wegst, 2004; for a review on functional materials in insects, see Schroeder et al., 2018). The diversity of the cuticle's mechanical properties (Politi et al., 2019; Hou et al., 2021) has its origin in cuticle thickness and microstructure, the abundance of proteins and water and the degree of tanning by quinone reactions (Andersen, 2010; Cribb et al., 2008a; Greenfeld et al., 2020; Hellenbrand & Penick, 2023; Hillerton & Vincent, 1982; Hopkins & Kramer, 1992; Hou et al., 2023; Li et al., 2020; Peisker et al., 2013; Schofield et al., 2002; for review on mechanical property gradients and their various origins, see Liu et al., 2017). Additionally, the chitin fibre density can be increased by the cross-linking transition metals copper (Cu), iron (Fe), manganese (Mn) and zinc (Zn) (Broomell et al., 2008; Cribb et al., 2008a; Cribb et al., 2008b; Degtyar et al., 2014; Hillerton & Vincent, 1982; Krings & Gorb, 2023; Kundanati et al., 2020; Kundanati & Gundiah, 2014; Lehnert et al., 2019; Lehnert et al., 2022; Politi et al., 2012; Pontin et al., 2007; Waite et al., 2004; see reviews by Liu et al., 2017; Politi et al., 2019). Besides, alkaline earth metals, such as calcium (Ca) and magnesium (Mg), can be incorporated into the cuticle increasing mechanical property values (Baio et al., 2019; Krings & Gorb, 2023; Leschen & Cutler, 1994; Polidori & Wurdack, 2019; Quicke et al., 2004; Vincent, 2002). With regard to ants and leaf-cutter ants, Zn was previously detected in the cuticle of the mandible cutting edge (Brito et al., 2017; Chowdhury & Rastogi, 2021; Dieterich & Betz, 2009; Edwards et al., 1993; Johnston et al., 2022; Schofield et al., 2002, 2003) and related to an increase in hardness and stiffness (Birkenfeld et al., 2024; Schofield et al., 2002).

The arthropod cuticle is composed of epi-, exo- and endocuticle and in some taxa of a mesocuticle, which is situated between the exo- and the endocuticle (see reviews by Hou et al., 2021; Politi et al., 2019). The outer epicuticle is cement-like, lacks a layered microstructure and consists of proteins and lipids and mainly serves as protection from desiccation. The exo-, meso- and endocuticles are

composed of chitin fibres and proteins (see review by Vincent & Wegst, 2004). The chitin fibrils are arranged in lamellar layers, which are densely packed in the exocuticle, whereas the endocuticle is rather hydrated and protein-rich (e.g. Hadley, 1986), which usually leads to a softer and more flexible endocuticle and a harder and stiffer exocuticle. The exocuticle tends to be more resistant to compressive stresses, but less to tension, whereas the endocuticle tends to be more resistant to tensile stresses, but less to compression. The mesocuticle, if present, connects these two layers and is less sclerotized than the exocuticle (see, e.g. Cheng et al., 2009). This aforementioned microstructure is typical for arthropods but can be altered depending on the selective pressure acting on the animal. In one study on a weevil experiencing high predatory pressure, the endocuticle was found to be sclerotized as well, resulting in higher *E* and *H* values and thus in stronger mechanical protection of the entire cuticle (Wang et al., 2019).

Since *Atta* ants of different castes perform different tasks and thus experience different selective pressures, it is likely that the mandibles not only differ in size, shape, and the mechanical properties of the exocuticle, but also in the mechanical parameters of the other cuticle layers. The here presented work aims at determining the cuticle layer properties and compositions of the minims and mediae *Atta laevigata* castes, as we found obvious differences between these two castes in the cuticle whereas the cuticle of the minors seemed to be a mixture of both castes. The data on the exocuticle was published before and here we add data on the meso- and endocuticle of the minims and mediae.

The workflow in this study was as follows. First, mandibles were embedded in the epoxy resin and polished. Then, the mandible layers were documented by scanning electron microscopy (SEM). Then, the mechanical properties (hardness, Young's modulus) were tested by the nanoindentation and the proportions of transition and alkaline earth metals were identified by the energy-dispersive X-ray spectroscopy (EDX) along the mandible's circumferential axis. As the mandibles, however, experience load along their longitudinal axis, the mechanical properties were also tested from this direction, which allows conclusions to be drawn about the degree of anisotropy of the cuticle material.

MATERIALS AND METHODS

Animals

Atta laevigata was kept in a colony of ~8000 individuals, which was originally ordered from the animal breeding facility (https://www.myants.de, Weiden, Germany) in 2020. Species identification was verified with the assistance of Professor Jonathan Z. Shik, University of Copenhagen, Denmark. For this study, only adult ants with fully hardened cuticles were used. The specimens were sorted into castes according to the literature (Arganda et al., 2020). We used the ants of two castes for this study. The specimens with a head of 0.9–1.1 mm were identified as minims and those with a width of 3.7–3.9 mm as mediae. The colony consisted of too few individuals to have soldiers (majors).

Five ants from each of the two castes were killed with chloroform, and their mandibles were extracted (Figure 1). The mandibles were cleaned with an ultrasonic cleaner (10 s) in 70% EtOH. The data on the exocuticle, tested in a circumferential direction, was previously published (Birkenfeld et al., 2024); here we add data on the meso- and endocuticle, as well as nanoindentation data obtained from testing in a longitudinal direction.

Preparation

The mandibles ($N = 20$; 5 individuals from each caste) were attached to glass slides with double-sided adhesive carbon pads. Around each mandible, a metallic ring was placed, which was then filled with epoxy resin (Reckli Epoxy WST; RECKLI GmbH, Herne, Germany). Polymerisation at room temperature took 3 days. Afterwards, the samples were polished with sandpaper to reach the cuticle regions of interest (see Figures 2a and 3a). With 1 µm aluminium oxide powder (Presi, 00120180; PRESI GmbH, Hagen, Germany) and a polishing plate on a polishing machine (Minitech 233/333; PRESI GmbH, Hagen, Germany), samples were smoothened. In an ultrasonic bath lasting 5 min, samples were cleaned in 70% EtOH from polishing powder.

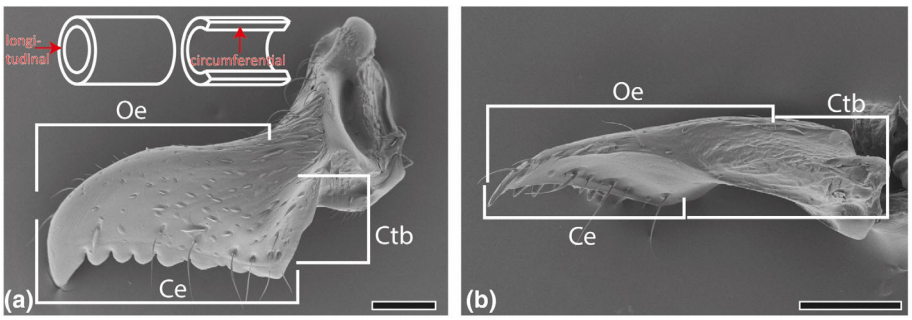

FIGURE 1 SEM image of one mandible from (a) media and (b) minim. Testing directions on the cuticle are shown in (a). The black arrow illustrates the longitudinal testing direction. The bubbles on the mandibles´ surfaces are artefacts as the coating does not stick to the entire surface. Scale bars: (a) 400 µm; (b) 120 µm. Ce, cutting edge; Ctb, curvature to basis; Oe, outer edge.

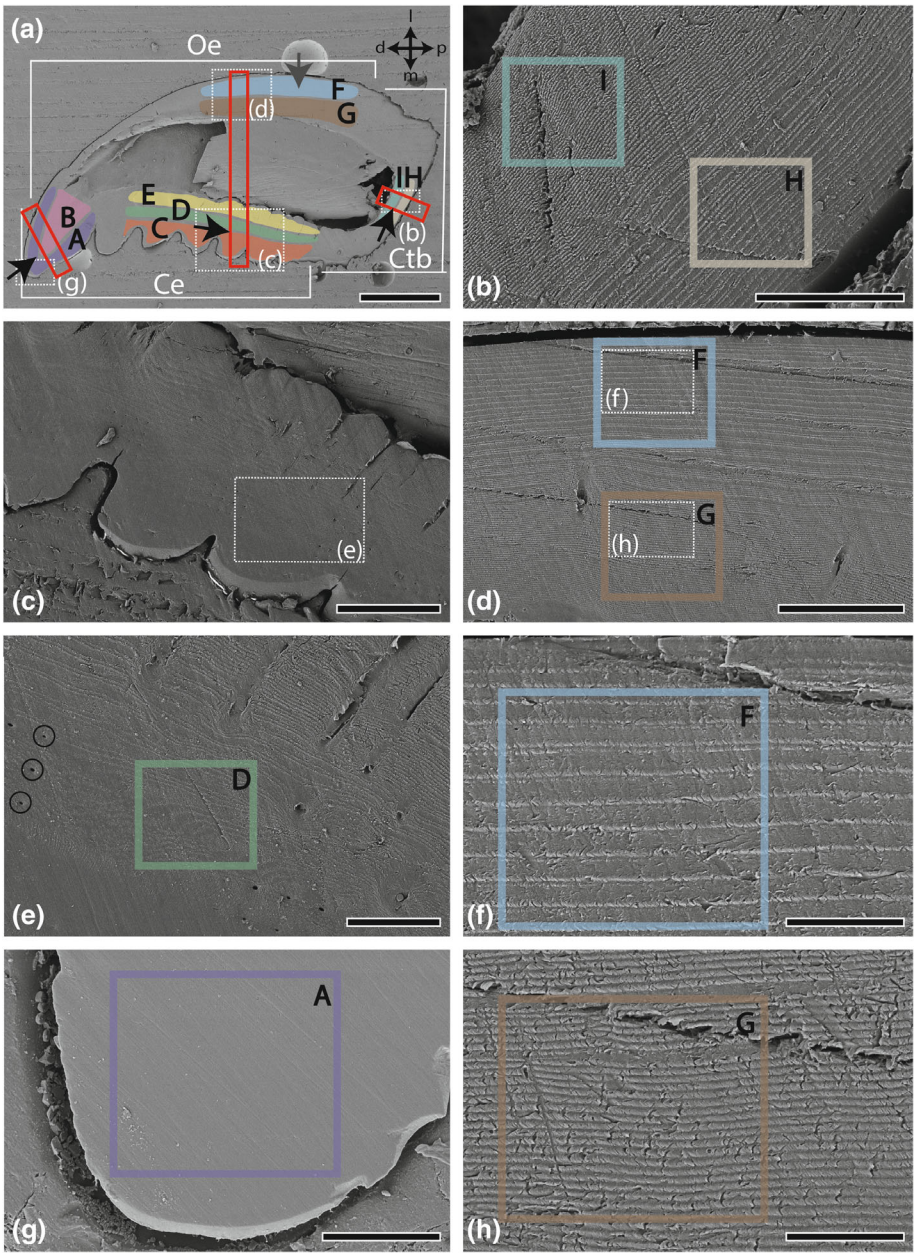

FIGURE 2 SEM images of one embedded and polished mandible from the media individual along its longitudinal axis (so that the localities could be tested in a circumferential direction). (a) Overview with highlighted regions of interest tested in this study. The colours and corresponding letters refer to the regions tested in a circumferential direction by EDX and nanoindentation (grey arrow). The red boxes highlight the regions of interest that were tested from a longitudinal direction (black arrows) by nanoindentation, after polishing along the longitudinal mandible axis. (b) Magnified region of the endocuticle (green) and the exocuticle (light brown) of the curvature to the basis. (c) Magnified region of the cutting edge. (d) Magnified region of the endocuticle (brown) and exocuticle (blue) of the outer edge. (e) Magnified region of the mesocuticle (light green) of the cutting edge. The circles highlight artefacts produced by EDX. (f) Magnified region of the exocuticle from the outer edge. (g) Magnified region of the exocuticle of the anterior tooth. (h) Magnified region of the endocuticle of the outer edge. Scale bars: (a) 300 µm; (b, e, g) 30 µm; (c) 80 µm; (d) 40 µm; (f, h) 10 µm. Ce, cutting edge; Ctb, curvature to the basis; d, dorsal; l, lateral; m, medial; Oe, outer edge; p, posterior.

Scanning electron microscopy

To document the layers of the cuticle, all polished samples were attached to SEM sample holders with double-sided adhesive carbon pads. The samples were sputter-coated with 5 nm platinum. A scanning electron microscope Zeiss LEO 1525 (One Zeiss Drive, Thornwood, United States) was employed for visualisation at 5 kV.

Energy-dispersive X-ray spectroscopy and nanoindentation

First, energy-dispersive X-ray spectroscopy (EDX/EDS) was performed. We used the Zeiss LEO 1525 equipped with an Octane Silicon Drift Detector (SDD) (Microanalysis system TEAM; EDAX Inc., Mahwah, United States). Samples were tested with the same settings

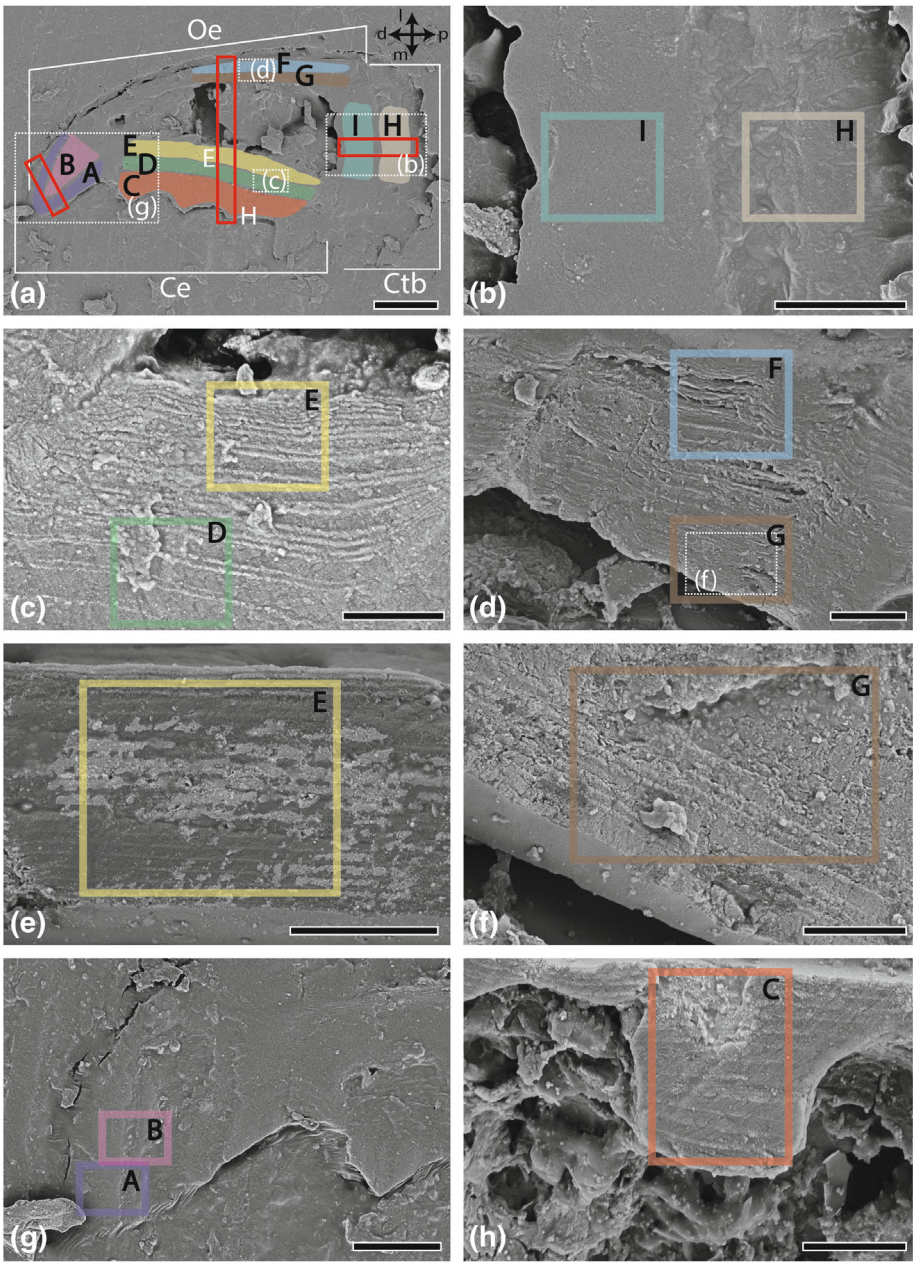

FIGURE 3 SEM images of one embedded and polished mandible from the minim individual along its longitudinal axis (so, that the localities could be tested in a circumferential direction). (a) Overview with highlighted regions of interest tested in this study. The colours and corresponding letters refer to the regions tested in a circumferential direction by EDX and nanoindentation. The red boxes highlight the regions of interest that were tested from a longitudinal direction by nanoindentation. (b) Magnified region of the endocuticle (green) and the exocuticle (light brown) of the curvature to the basis. (c) Magnified region of the endocuticle (yellow) and the mesocuticle (light green) of the cutting edge. (d) Magnified region of the endocuticle (brown) and exocuticle (blue) of the outer edge. (e) Magnified region of the endocuticle of the cutting edge from another specimen. (f) Magnified region of the exocuticle from the outer edge. (g) Magnified region of the exocuticle of the anterior tooth. (h) Magnified region of the exocuticle of the fourth tooth from another specimen. Scale bars: a, 60 μm; b, G, 30 μm; c, D, H, 8 μm; e, 10 μm; f, 2 μm. Ce, cutting edge; Ctb, curvature to the basis; d, dorsal; l, lateral; m, medial; Oe, outer edge; p, posterior.

(acceleration voltage of 20 kV, working distance 15 mm, lens aperture 60 μm, measurement time for each measurement point 30 s, resolution 137.6 eV) following previous protocols (Birkenfeld et al., 2024; Krings, Brütt, et al., 2022; Krings, Matsumura, et al., 2022). Cu was used for calibration. Small areas with sizes between 2×2 and 10×10 μm were analysed. We detected these elements and recorded their proportions: aluminium (Al), carbon (C), calcium (Ca), sodium (Cl), copper (Cu), fluorine (F), iron (Fe), potassium (K), magnesium (Mg), manganese (Mn), nitrogen (N), sodium (Na), oxygen (O), phosphorus (P), platinum (Pt), sulphur (S), silicon (Si) and zinc (Zn). We included only tests with peaks that were higher than the noise. Some elements were measured, but not included in the discussion, because they are part of chitin and the associated proteins (H, C, N, O) or could be artefacts from the polishing paste (Al, O). P and Pt (from the

sputter coating) had to be discussed together because their peaks overlap and the EDX cannot differentiate the elements. A platinum coating was, however, necessary to see if the measurement was reliable (i.e. if P + Pt was found in very high proportions, e.g. >5 atomic %, this one measurement was excluded from the results). For discussion, Ca, Cl, Cu, F, Fe, K, Mg, Mn, Na, P, Pt, S, Si, and Zn were summarized to 'All Elements, Ae'.

Then, nanoindentation was performed with the same samples and at the same regions in a circumferential direction (along the length of the mandible; terminology of testing direction after Li et al., 2020). They were attached to the sample holders following established protocols (Krings, Brütt, et al., 2022; Krings, Matsumura, et al., 2022). Each region of interest was tested at room temperature with an SA2 nanoindenter (MTS Nano Instruments, Oak Ridge, United States) with a Berkovich diamond tip and a dynamic contact module (DCM) head was utilized. Nanoindentation tip calibration was performed with glass and the resulting force/displacement curves were stable in the depth from 150 to 1500 nm (which was the end of the test). The Young's modulus (*E*) was calculated via the Oliver–Pharr method (Oliver & Pharr, 1992). Hardness (*H*) and *E* were determined from force-distance curves using the continuous stiffness mode (CSM). The Poisson's ratio was set to 0.3 and the allowable drift rate to 0.1 nm/s. All tests were conducted under normal room conditions (relative humidity 28%–30%, temperature 22–24°C), with each indent and corresponding curve manually controlled. Due to the Pt sputter coating, *E* and *H* were determined at penetration depth ranging from 600 to 800 nm. Approximately 40 values were obtained from this indentation depth for each site, which was then averaged to calculate one mean *H* and one mean *E* value per indent.

For circumferential direction (with the mandible polished along its longitudinal axis), overall 1200 localities were tested (thereof 450 from minims and 750 from mediae) and 1178 by EDX (thereof 376 from minims and 802 from mediae; see Tables S1 and S2 for the number of measurements for each region, locality, cuticle layer and caste).

Afterwards, samples were detached from sample holders. Then, the metallic ring was removed by a metal cutter, the samples were turned to 90°, polished and smoothened to test the regions of interest from the longitudinal direction by nanoindentation (with the mandible polished along its transversal or circumferential axis; terminology of testing direction after Li et al., 2020). To achieve a statistically relevant number of measurements, the sample was smoothened (a few micrometres) after one first round of nanoindentation to test it again in a second and then a third round and so on. Overall, 1480 localities were tested by nanoindentation (thereof 443 from minims and 1037 from mediae; see Table S1 for the number of measurements for each region, locality, cuticle layer, and caste).

Statistics

All analyses were performed with JMP Pro, Version 14 (SAS Institute Inc., Cary, United States). For normality testing, a Shapiro–Wilk *W*-test was run. The data were not normally distributed. Afterwards, pairwise comparisons by Steel-Dwass, which corrects for the nested structure of the data, were performed.

Correlation coefficients of *E* and *H* values were calculated with JMP. *F*-tests (Levene test) were performed to test for the equality of coefficients of variation.

Since EDX and nanoindentation sample sizes are not the same, no correlation coefficients for elemental content and mechanical properties could be calculated. Thus, the content of the individual elements and the mechanical properties of each region were calculated (mean and standard deviation) and then plotted with Excel, version 16.0 (Microsoft Corporation, Redmond, United States). Here, a trend line was added to each plot. This was done for the circumferential direction, as for this axis we performed EDX and nanoindentation tests.

RESULTS

Cuticle layers

In the outer edge (region G), the curvature to the basis (region I) and the cutting edge (region E) of the mediae, the inner chitin fibres (of, i.e. the endocuticle) were oriented in both longitudinal and circumferential directions (for longitudinal axis, see Figure 2b,d,e,h; for circumferential axis, see Figure 3d,e). In contrast, the fibres of the outer chitin layer (of, i.e. the exocuticle) were mostly oriented longitudinally in the outer edge (region F) and the curvature to the basis (region H) (for longitudinal axis, see Figure 2b,d,f; for circumferential axis, see Figure 3e). In the cutting edge, the endocuticle (region E) was surrounded by chitin fibres (of, i.e. the mesocuticle), which were mostly oriented in a longitudinal direction (region D), and very small and dense fibres (of, i.e. the exocuticle), which seemed rather homogeneous (region C) (for longitudinal direction, see Figure 2c,e; for circumferential direction, see Figure 3e). The anterior tooth (regions A and B) seemed to be composed of rather homogeneous material, which consisted of very small and dense fibres (for longitudinal direction, see Figure 2g; for circumferential direction, see Figure 3a).

In the minims, we could determine a trend similar with regard to the microstructure of the cutting edge and the outer edge (see Figure 4). However, the curvature to the basis (regions I and H) seemed to be denser and to contain smaller fibres (see Figure 4b).

Elemental composition

Elemental composition was tested along the circumferential axis. As described previously (Birkenfeld et al., 2024), the mediae contained significantly higher content of Ae (sum of Ca, Cl, Cu, Fe, K, Mg, Mn, P + Pt, S, Si, Zn), K, Mn, Si and Zn than the minims (see Table S3 for values and Figure S1).

In both castes, the highest Zn content was determined for the exocuticle of the mandible cutting edge (regions A, B, C; see Table S3 for values and Tables S4 and S5 for *p*-values). In the mediae, the

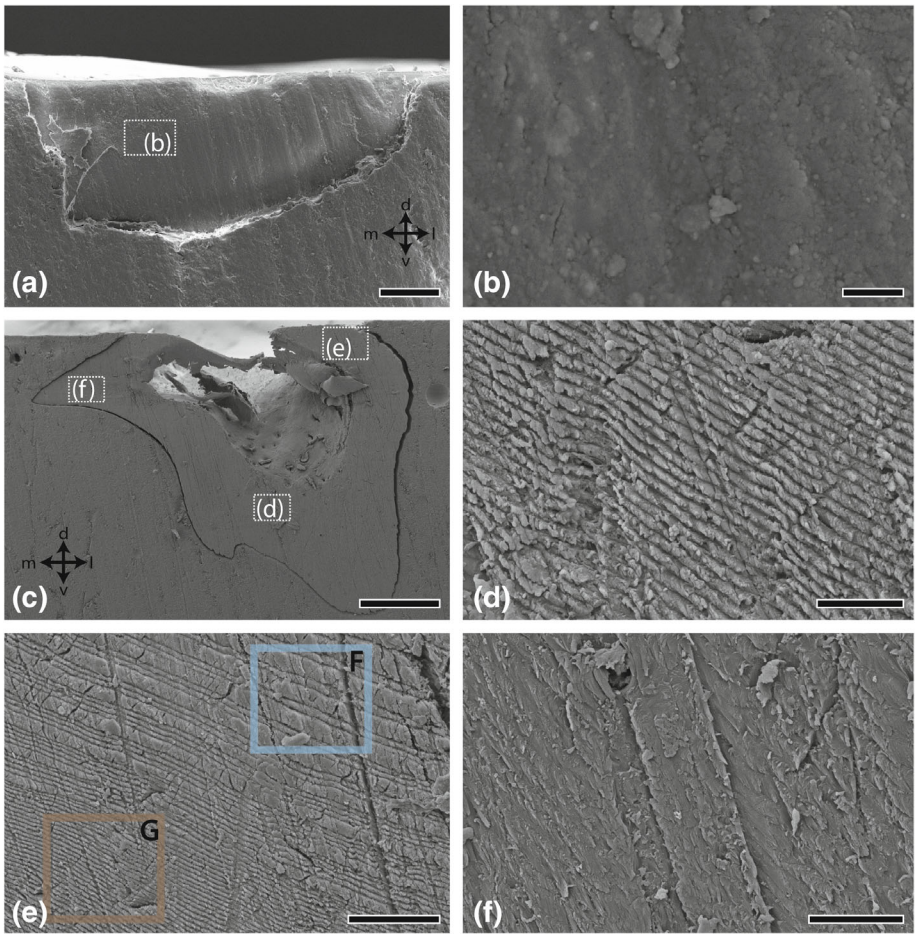

FIGURE 4 SEM images of one embedded and polished mandible from the media individual along its circumferential axis (so, that the localities could be tested in longitudinal direction). (a) View on the anterior tooth with (b) magnification of its exocuticle. (c) View on the circumferential axis near the fifth tooth. (d) Magnified region of the endocuticle. (e) Magnified region of the endocuticle (brown) and exocuticle (blue) of the outer edge from another specimen. (f) Magnified region of the mesocuticle from the cutting edge. Scale bars: (a) 30 µm; (b) 1 µm; (c) 200 µm; (d) 4 µm; (e, f) 8 µm. d, dorsal; l, lateral; m, medial; p, posterior.

mesocuticle contained significantly more Zn than the exocuticle of the outer edge, the exocuticle of the curvature to the basis and the endocuticle, which contained the smallest amount of Zn (see Tables S3 and S4). In the minims, the mesocuticle, the exocuticle of the outer edge, the exocuticle of the curvature to the basis, and the endocuticle contained small amounts of Zn (see Tables S3 and S5). For each caste, most localities showed significant or highly significant differences with regard to the content of Ae, Ca, Cl, Cu, Fe, K, Mg, Mn, S, Si and Zn (see Tables S4 and S5 for *p*-values).

Mechanical properties

E and *H* were very strongly correlated with a correlation coefficient of 0.89 ($p < 0.0001^*$). The cuticle layers differed highly significantly between the mediae and the minims—regardless of the testing direction (see Figure 5 and Figure S2 for significances).

In the mediae, the exocuticle was, regardless of the direction of nanoindentation tests, harder and stiffer than the endocuticle (see Figures 5 and 6, Figure S2 and Table S6 for values). When tested from the longitudinal, the exocuticle and mesocuticle were highly significantly harder and stiffer than when tested from the circumferential direction (see Figures 5 and 6, Figure S2, and Table S7 for *p*-values). Tested in a circumferential direction, the endocuticle was harder and stiffer than the mesocuticle. When indented from a longitudinal direction, the endocuticle was the softest and most flexible component of the cuticle layers (see Figures 5 and 6, Figure S2 and Tables S6 and S7). For the endocuticle, results of *E* and *H* were, except for locality G showing significant differences, not different (see Table S8 for *p*-values). The mesocuticle was significantly harder and stiffer when tested from a longitudinal than from a circumferential direction (see Figure 6 and Table S7 for *p*-values).

In the minims, the mesocuticle was significantly harder and stiffer than the exo- and endocuticle, when tested in a circumferential direction (see Figures 5 and 6, Figure S2 and Table S7 for *p*-values). Here, the exocuticle was the softest and most flexible region. When tested from a longitudinal direction, the three cuticle layers did not show differences with regard to *E* and *H* values (see Figures 5 and 6 and Figure S2).

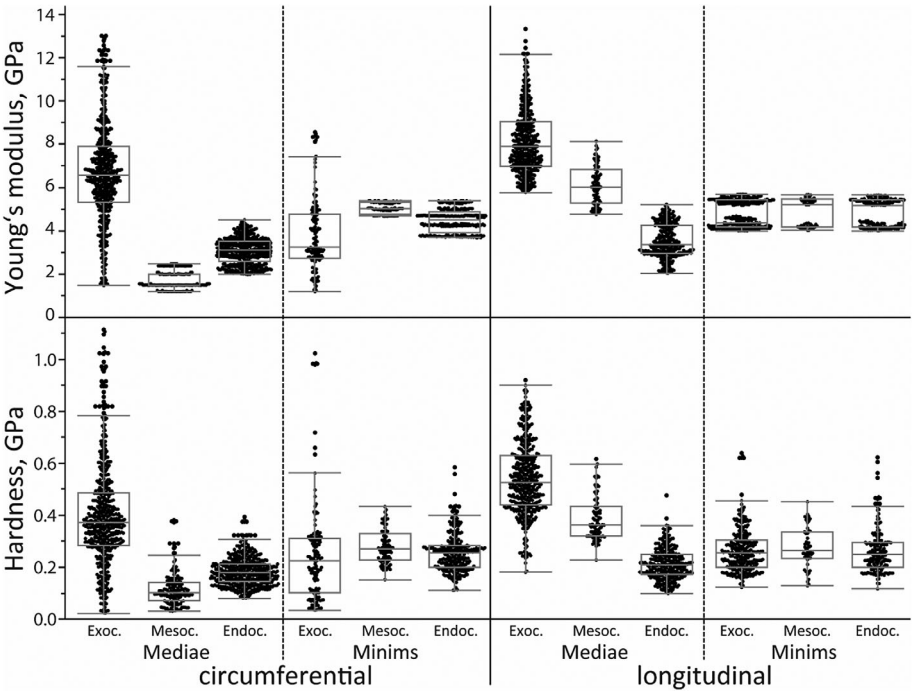

FIGURE 5 Young's modulus *E* and Hardnesss *H* values, both given in GPa, for each cuticle layer of the two castes, were tested in circumferential and longitudinal directions. For statistical results, see Figure S2. Circumferential, along the circumference of the mandible; longitudinal, along the length of the mandible.

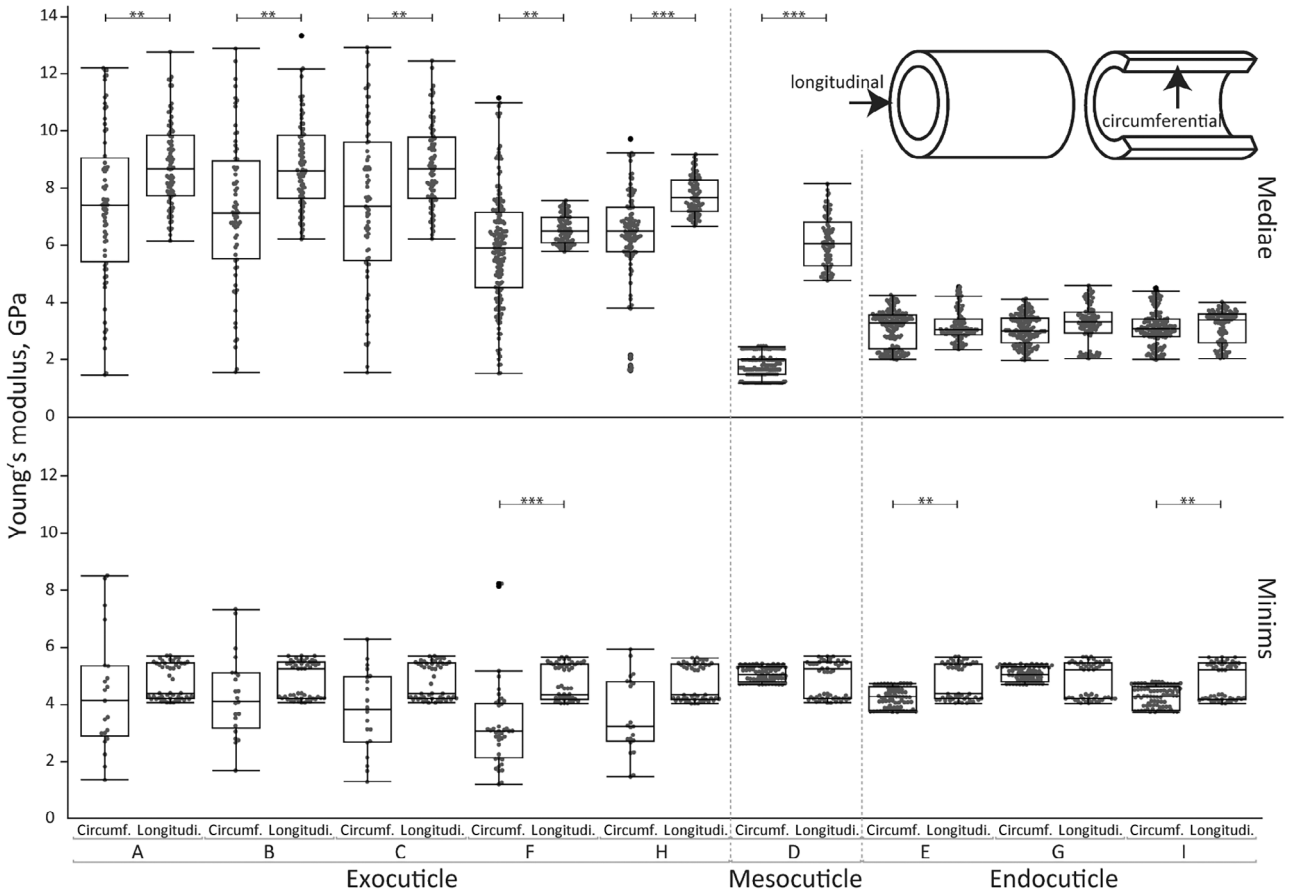

FIGURE 6 Young's modulus (*E*) values, given in GPa, for each region of interest of the two castes. The statistical results are from pairwise comparisons between the two testing directions (longitudinal and circumferential). Circumferential, along the circumference of the mandible; longitudinal, along the length of the mandible. circumf., circumferential; longitudi., longitudinal.

The region g of the exocuticle and the mesocuticle were harder and stiffer than most regions (a, c, f, h) of the exocuticle, regardless of the direction of nanoindentation tests (see Figure 6 and Table S8 for *p*-values). When tested from longitudinal, most regions (b, c, f, h) of the exocuticle were significantly harder and stiffer, when tested from a circumferential direction. For the mesocuticle, no differences were determined (see Figure 6 and Table S8 for *p*-values). In the endocuticle, the regions e and i were highly significantly harder and stiffer, when tested from longitudinal direction.

When the regions tested from the same direction were compared within the mediae, it was found that they were mostly highly significantly or significantly different for both *E* and *H* (see Figure 5, Figure S2 and Table S9 for *p*-values). Only the regions of the endocuticle and some of the exocuticle did not differ. In the minims, most regions were not different with regard to both parameters (see Figure 5, Figure S2 and Table S9 for *p*-values).

F-test revealed that the variability of *E* and *H* of minims and mediae were highly significantly different—regardless of the testing direction (df: 1, *p*-values always <0.0001*).

Relationships between parameters

As described in Birkenfeld et al. (2024), *H* and *E* showed a clear relationship with the content of Ca, Cl, Cu, Fe, Mg, Mn, Si and Zn along the circumferential axis (see Figures S2–S17, respectively).

Additionally, we found that the mandible cuticle was harder and stiffer when most fibres were oriented parallel to the indentation direction: in the exocuticle, testing from a longitudinal direction always leads to the higher *E* and *H* values. Here, most chitin fibres run along the longitudinal axis. In the mesocuticle, *E* and *H* values were also higher, when tested from longitudinal direction. Here, most fibres also run along the longitudinal axis.

The *E* and *H* values of the endocuticle were rather similar when tested from longitudinal and circumferential directions. Here we found, that similar quantities of the chitin bundles were oriented in the circumferential and the longitudinal direction.

DISCUSSION

Cuticle structure and mechanical properties

Chitin bundle orientation directly relates to the loading condition of the respective region (for review, see Politi et al., 2019). A twisted plywood architecture (structural isotropy) with the orientation of the chitin bundles gradually varying, which is common in arthropod cuticles, relates to mechanical plane isotropy as an adaptation to stresses from all in-plane sides (see, e.g. Greenfeld et al., 2020). A more unidirectional fibre orientation architecture (i.e. structural anisotropy) is related to stresses preferably acting along one axis (along the bundles).

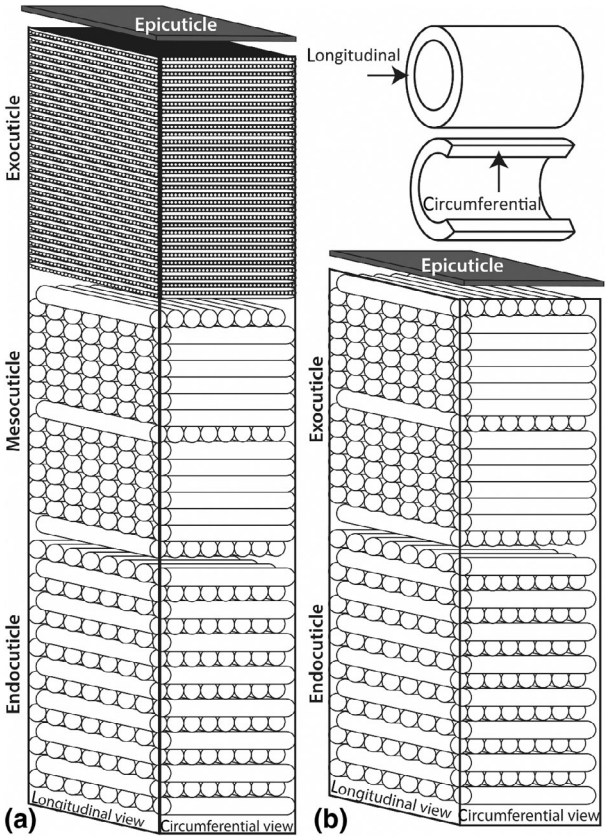

FIGURE 7 Schematic illustration from the longitudinal and circumferential view of the cuticle microstructure from (a) the cutting edge and (b) the outer edge and the curvature to the basis. Please note that we were not able to identify the twisted plywood structure of individual chitin fibres and the precise orientation of the fibres, but rather the orientation of larger bundles, as far as we can identify this from the SEM image. Thus, this scheme is not comprehensive but limited due to our methodology. Circumferential, along the circumference of the mandible; longitudinal, along the length of the mandible.

To determine the precise chitin bundle orientation, different methods, such as synchrotron X-ray diffraction measurements (see, e.g. Zhang et al., 2016), are necessary. From SEM observation, we can only deduce the very broad orientation of some larger bundles, but without knowledge about the sizes and quantities of pitches or the precise angles of the fibres. Thus, our diagram of the cuticle layers in the mandibles (see Figure 7) is rather rough, but we decided to include it in our manuscript to help the reader to judge the material architecture at least to some degree.

In general, we found that the endocuticle and the exocuticle of the cutting edge seem to be structurally isotropic as most fibres seem to be oriented in different directions (see Figure 7). This indicates that stresses from all in-plane sides act on these layers. The mesocuticle, which can be found in the mandible cutting edge, as well as the exocuticle on the outer edge and the curvature to the basis, seem to be mostly composed of fibre bundles, which run along the longitudinal axis of the mandible (structural anisotropy; see Figure 7). This

indicates that these fibres rather experience stresses along their longitudinal axis.

As already described (Birkenfeld et al., 2024; Brito et al., 2017; Edwards et al., 1993; Johnston et al., 2022; Schofield et al., 2002), the Zn content of *Atta* mandibles is directly related to the mechanical property values (*E* and *H*). This element was, however, only determined in the exocuticle of the mandibles' cutting edges and can thus not cause the mechanical property differences between the endo-, mesocuticle as well as the exocuticle of the outer edge and the curvature to the basis. Thus, its origins could lay in either the chitin bundle architecture or the degree of sclerotisation of the protein matrix.

In general, we detected that, when the nanoindentation direction aligns parallel to the bundles (e.g. the mesocuticle in a longitudinal direction), *E* and *H* values are higher than when they are tested perpendicularly (e.g. the exocuticle of the curvature to the basis or the outer edge in circumferential direction). This is similar to the situation previously described in gastropod radular teeth, where mechanical property values have been found to increase when the mineral rods are tested in a parallel direction (de Obaldia et al., 2015). The orientation of the rods together with the chitin fibres probably reduces crack initiation and wear (de Obaldia et al., 2016; Grunenfelder et al., 2014; Joester & Brooker, 2016; van der Wal et al., 1999; Weaver et al., 2010). This is also similar to the cuticle of locust, where *E* and *H* values increase when the fibres are tested parallel (Li et al., 2020). In the exocuticle of the mandible cutting edge, we determined smaller bundles in comparison to the rest of the cuticle. This is again similar to the situation in radular teeth, where high quantities of smaller fibres can be found in the interacting regions (Wang et al., 2018). Here, each fibre serves as a nucleation site and with an increasing number of fibres, the number of mineral rods increases – leading to an increased resistance to tensile stress, because of their reduced brittleness. In the here studied exocuticle of the ant mandible cutting edge, helical structures or twisted-ply structures could be present, as this is often found on exterior surfaces to increase strength and toughness in multiple directions and to create in-plane isotropy (see Aizenberg et al., 2005; Bouligand, 1972; Khayer Dastjerdi & Barthelat, 2015; Lenau & Barfoed, 2008; Nikolov et al., 2011; Weaver et al., 2007; Weaver et al., 2012; Yamamoto et al., 2012; Yang et al., 2014; Zimmermann et al., 2013; for reviews see Naleway et al., 2015; Zhang et al., 2022).

When the two castes are compared, it was found that the *E* and *H* values of the cuticular layers are rather similar in the minims, whereas the exo-, meso, and endocuticles are significantly different in the mediae. The mandibles of the mediae have additionally a wider range of *E* and *H* values, whereas the cuticular layers of the minims seem rather homogeneous. This indicates that the mandibles of the mediae experience higher stresses than those of the minims, as the soft and flexible mesocuticle acts as a cushion to adjust to compressive stresses, whereas the stiff and hard exocuticle acts as resistance against tensile stresses. This can be directly related to the task performance as mediae cut tough plant material, whereas the minims care for the fungus and the brood, which does not involve high stresses or loads. The direct relationship between ant size and forces generated by the mandibles was previously experimentally determined (Püffel, Roces, et al., 2023), which supports our interpretation.

With regard to the anisotropy of the mechanical parameters (*E* and *H*), we determined that the mediae show a higher degree of anisotropy than the minims. This indicates that the mandibles of the mediae experience rather anisotropic stresses, probably along their longitudinal axis as most fibres are oriented along this. This would be the case when plant material is cut with the mandibular cutting edge or during transportation. The mandibles of minims seem to experience rather isotropic stresses.

When the microstructures or the representatives of the two castes are, however, compared in SEM, we found that the microstructures of the mandibles seem to be rather similar. General similarities in the cuticle microstructure of different ant species have been previously already documented (Barlow et al., 2019), which indicates that there is presumably a general pattern. The differences between the two castes in the mechanical properties could potentially be explained with different compositions of the protein matrix of the two castes, which, depending on the proteins involved can either increase or decrease *E* and *H* values (see, e.g. Montroni et al., 2021). This, however, awaits further investigation.

AUTHOR CONTRIBUTIONS

Wencke Krings: Conceptualization; investigation; funding acquisition; writing – original draft; validation; methodology; visualization; project administration; software; data curation; supervision. **Valentin Birkenfeld:** Investigation; writing – review and editing; formal analysis; resources; methodology; software. **Stanislav N. Gorb:** Conceptualization; writing – review and editing; methodology; validation; project administration; supervision; resources.

ACKNOWLEDGEMENTS

We would like to thank Jonathan Z. Shik, University of Copenhagen, Denmark, for his support in species identification, Elke Woelken, Institute of Cell and Systems Biology of Animals, Universität Hamburg, Germany, for her support with the SEM and Alexander Kovalev, Christian-Albrechts-Universität zu Kiel, Germany, for his support with the nanoindentation. We are thankful for the constructive comments of the anonymous reviewers and the editorial office. Open Access funding enabled and organized by Projekt DEAL.

FUNDING INFORMATION

No specific funding was received.

CONFLICT OF INTEREST STATEMENT

The authors declare no conflicts of interest.

DATA AVAILABILITY STATEMENT

All results can be found in the Supplementary Material.

ETHICS STATEMENT

Not applicable.

USE OF ARTIFICIAL INTELLIGENCE (AI) AND AI-ASSISTED TECHNOLOGIES

No AI was used.

ORCID

Wencke Krings https://orcid.org/0000-0003-2158-9806

REFERENCES

Aizenberg, J., Weaver, J.C., Thanawala, M.S., Sundar, V.C., Morse, D.E. & Fratzl, P. (2005) Skeleton of *Euplectella* sp.: structural hierarchy from the nanoscale to the macroscale. *Science*, 309, 275–278.

Andersen, S.O. (2010) Insect cuticular sclerotization: a review. *Insect Biochemistry and Molecular Biology*, 40, 166–178.

Arganda, S., Hoadley, A.P., Razdan, E.S., Muratore, I.B. & Traniello, J.F.A. (2020) The neuroplasticity of division of labor: worker polymorphism, compound eye structure and brain organization in the leafcutter ant *Atta cephalotes*. *Journal of Comparative Physiology. A, Neuroethology, Sensory, Neural, and Behavioral Physiology*, 206, 651–662.

Baio, J.E., Jaye, C., Sullivan, E., Rasmussen, M.H., Fischer, D.A., Gorb, S.N. et al. (2019) NEXAFS imaging to characterize the physiochemical composition of cuticle from African flower scarab *Eudicella gralli*. *Nature Communications*, 10, 4758.

Barbakadze, N., Enders, S., Gorb, S.N. & Arzt, E. (2006) Local mechanical properties of the head articulation cuticle in the beetle *Pachnoda marginata* (Coleoptera, Scarabaeidae). *Journal of Experimental Biology*, 209, 722–730.

Barlow, M.M., Bicknell, R.D.C. & Andrew, N.R. (2019) Cuticular microstructure of Australian ant mandibles confirms common appendage construction. *Acta Zoologica*, 101, 260–270.

Birkenfeld, V., Gorb, S.N. & Krings, W. (2024) Mandible elemental composition and mechanical properties from distinct castes of the leafcutter ant *Atta laevigata* (Attini; Formicidae). *Interface Focus*, 14, 20230048.

Bouligand, Y. (1972) Twisted fibrous arrangements in biological materials and cholesteric mesophases. *Tissue and Cell*, 4, 189–217.

Brito, T.O., Elzubair, A., Araújo, L.S., Camargo, S.A.S., Souza, J.L.P. & Almeida, L.H. (2017) Characterization of the mandible *Atta laevigata* and the bioinspiration for the development of a biomimetic surgical clamp. *Materials Research*, 20, 1525–1533.

Broomell, C.C., Chase, S.F., Laue, T. & Waite, J.H. (2008) Cutting edge structural protein from the jaws of Nereis virens. *Biomacromolecules*, 9, 1669–1677.

Cahan, S.H. & Fewell, J.H. (2004) Division of labor and the evolution of task sharing in queen associations of the harvester ant *Pogonomyrmex californicus*. *Behavioral Ecology and Sociobiology*, 56, 9–17.

Chen, Y.H., Skote, M., Zhao, Y. & Huang, W.M. (2013) Stiffness evaluation of the leading edge of the dragonfly wing via laser vibrometer. *Materials Letters*, 97, 166–168.

Cheng, L., Wang, L. & Karlsson, A.M. (2009) Mechanics-based analysis of selected features of the exoskeletal microstructure of *Popillia japonica*. *Journal of Materials Research*, 24, 3253–3267.

Cherrett, J.M. (2019) History of the leaf-cutting ant problem. In: Clifford, S.L. (Ed.) *Fire ants and leaf-cutting ants*. Florida: CRC Press, pp. 10–17.

Chowdhury, R. & Rastogi, N. (2021) Comparative analysis of mandible morphology in four ant species with different foraging and nesting habits. *bioRxiv* https://doi.org/10.1101/2021.08.26.457866

Cribb, B.W., Stewart, A., Huang, H., Truss, R., Noller, B., Rasch, R. et al. (2008a) Insect mandibles—comparative mechanical properties and links with metal incorporation. *The Science of Nature*, 95, 17–23.

Cribb, B.W., Stewart, A., Huang, H., Truss, R., Noller, B., Rasch, R. et al. (2008b) Unique zinc mass in mandibles separates drywood termites from other groups of termites. *The Science of Nature*, 95, 433–441.

de Obaldia, E.E., Herrera, S., Grunenfelder, L.K., Kisailus, D., & Zavattieri, P. (2016). Competing mechanisms in the wear resistance behavior of biomineralized rod-like microstructures. *Journal of the Mechanics and Physics of Solids*, 96, 511–534. https://doi.org/10.1016/j.jmps.2016.08.001

de Obaldia, E.E., Jeong, C., Grunenfelder, L.K., Kisailus, D. & Zavattieri, P. (2015) Analysis of the mechanical response of biomimetic materials with highly oriented microstructures through 3D printing, mechanical testing and modeling. *Journal of the Mechanical Behavior of Biomedical Materials*, 48, 70–85.

Degtyar, E., Harrington, M.J., Politi, Y. & Fratzl, P. (2014) The mechanical role of metal ions in biogenic protein-based materials. *Angewandte Chemie International Edition*, 53, 12026–12044.

Dieterich, A. & Betz, O. (2009) Elementsensitive Synchrotron-Mikrotomographie zur Darstellung von Zinkeinlagerungen in den Mandibeln ausgewählter Insekten. *Mitteilungen der Deutschen Gesellschaft für Allgemeine und Angewandte Entomologie*, 17, 285–288.

Dirks, J.H. & Taylor, D. (2012) Veins improve fracture toughness of insect wings. *PLoS One*, 7, e43411.

Edwards, A.J., Fawke, J.D., McClements, J.G., Smith, S.A. & Wyeth, P. (1993) Correlation of zinc distribution and enhanced hardness in the mandibular cuticle of the leaf-cutting ant *Atta sexdens rubropilosa*. *Cell Biology International*, 17, 697–698.

Greenfeld, I., Kellersztein, I. & Wagner, H.D. (2020) Nested helicoids in biological microstructures. *Nature Communications*, 11, 224.

Grunenfelder, L.K., de Obaldia, E., Escobar, Wang, Q., Li, D., Weden, B., Salinas, C. et al. (2014) Stress and damage mitigation from oriented nanostructures within the radular teeth of *Cryptochiton stelleri*. *Advanced Functional Materials*, 24, 6093–6104.

Hadley, N.F. (1986) The arthropod cuticle. *Scientific American*, 255, 104–113.

Hayot, C.M., Enders, S., Zera, A. & Turner, J.A. (2013) Nanoindentation to quantify the effect of insect dimorphism on the mechanical properties of insect rubberlike cuticle. *Journal of Materials Research*, 28, 2650–2659.

Hellenbrand, J.P. & Penick, C.A. (2023) Ant cuticle microsculpturing: diversity, classification, and evolution. *Myrmecological News*, 33, 123–138.

Hillerton, J.E. & Vincent, J.F.V. (1982) The specific location of zinc in insect mandibles. *Journal of Experimental Biology*, 101, 333–336.

Hopkins, T.L. & Kramer, K.J. (1992) Insect cuticle sclerotization. *Annual Review of Entomology*, 37, 273–302.

Hou, F., Gong, Z., Jia, F., Cui, W., Song, S., Zhang, J. et al. (2023) Insights into the relationships of modifying methods, structure, functional properties and applications of chitin: a review. *Food Chemistry*, 409, 135336.

Hou, J., Aydemir, B.E. & Dumanli, A.G. (2021) Understanding the structural diversity of chitins as a versatile biomaterial. *Philosophical Transactions of the Royal Society A*, 379, 20200331.

Joester, D. & Brooker, L.R. (2016) The chiton radula: a model system for versatile use of iron oxides*. In: Faivre, D. (Ed.) *Iron oxides: from nature to applications*. Weinheim: Wiley-VCH Verlag GmbH & Co. KGaA, pp. 177–206.

Johnston, R.E., Said, M.W., Labonte, D., Russell, J., Sackett, E. & Board, R. (2022) Correlative structure-property characterisation of the leafcutter ant (*Atta cephalotes*) mandible. *Microscopy and Microanalysis*, 28, 1342–1346.

Khayer Dastjerdi, A. & Barthelat, F. (2015) Teleost fish scales amongst the toughest collagenous materials. *Journal of the Mechanical Behavior of Biomedical Materials*, 52, 95–107.

Klocke, D. & Schmitz, H. (2011) Water as a major modulator of the mechanical properties of insect cuticle. *Acta Biomaterialia*, 7, 2935–2942.

Klunk, C.L., Argenta, M.A., Casadei-Ferreira, A., Economo, E.P. & Pie, M.R. (2021) Mandibular morphology, task specialization and bite

mechanics in *Pheidole* ants (Hymenoptera: Formicidae). *Journal of the Royal Society Interface*, 18, 20210318.

Klunk, C.L., Argenta, M.A., Casadei-Ferreira, A. & Pie, M.R. (2023) Mechanical demands of bite in plane head shapes of ant (Hymenoptera: Formicidae) workers. *Ecology and Evolution*, 13, e10162.

Klunk, C.L., Argenta, M.A., Rosumek, F.B., Schmelzle, S., van de Kamp, T., Hammel, J.U. et al. (2023) Simulated biomechanical performance of morphologically disparate ant mandibles under bite loading. *Scientific Reports*, 13, 16833.

Krings, W., Brütt, J.-O. & Gorb, S.N. (2022) Ontogeny of the elemental composition and the biomechanics of radular teeth in the chiton *Lepidochitona cinerea*. *Frontiers in Zoology*, 19, 19.

Krings, W. & Gorb, S.N. (2023) Mechanical properties of larval mouthparts of the antlion *Euroleon nostras* (Neuroptera: Myrmeleontidae) and their correlation with cuticular material composition. *Zoomorphology*, 142, 423–438.

Krings, W., Matsumura, Y., Brütt, J.-O. & Gorb, S.N. (2022) Material gradients in gastropod radulae and their biomechanical significance: a combined approach on the paludomid *Lavigeria grandis*. *The Science of Nature*, 109, 52.

Kundanati, L., Chahare, N.R., Jaddivada, S., Karkisaval, A.G., Sridhar, R., Pugno, N.M. et al. (2020) Cutting mechanics of wood by beetle larval mandibles. *Journal of the Mechanical Behavior of Biomedical Materials*, 112, 104027.

Kundanati, L., Das, P. & Pugno, N.M. (2021) Prey capturing dynamics and nanomechanically graded cutting apparatus of dragonfly nymph. *Materials*, 14, 559.

Kundanati, L. & Gundiah, N. (2014) Biomechanics of substrate boring by fig wasps. *Journal of Experimental Biology*, 217, 1946–1954.

Leal, I.R. & Oliveira, P.S. (2000) Foraging ecology of attine ants in a Neotropical savanna: seasonal use of fungal substrate in the cerrado vegetation of Brazil. *Insectes Sociaux*, 47, 376–382.

Lehnert, M.S., Lanba, A., Reiter, K.E., Fonseca, R.J., Minninger, J., Hall, B. et al. (2022) Mouthpart adaptations of antlion larvae facilitate prey handling and fluid feeding in sandy habitats. *Journal of Experimental Biology*, 225, jeb244220.

Lehnert, M.S., Reiter, K.E., Smith, G.A. & Kritsky, G. (2019) An augmented wood-penetrating structure: cicada ovipositors enhanced with metals and other inorganic elements. *Scientific Reports*, 9, 19731.

Lenau, T. & Barfoed, M. (2008) Colours and metallic sheen in beetle shells—a biomimetic search for material structuring principles causing light interference. *Advanced Engineering Materials*, 10, 299–314.

Leschen, R.A.B. & Cutler, B. (1994) Cuticular calcium in beetles (Coleoptera, Tenebrionidae, Phrenapetinae). *Annals of the Entomological Society of America*, 87, 918–921.

Li, C., Gorb, S.N. & Rajabi, H. (2020) Cuticle sclerotization determines the difference between the elastic moduli of locust tibiae. *Acta Biomaterialia*, 103, 189–195.

Li, C., Gorb, S.N. & Rajabi, H. (2022) Effect of sample treatment on the elastic modulus of locust cuticle obtained by nanoindentation. *Beilstein Journal of Nanotechnology*, 13, 404–410.

Li, C., Rajabi, H. & Gorb, S.N. (2022) Conflicting requirements for transparency and mechanical stability in the compound eyes of desert locusts. *Advanced Materials Interfaces*, 9, 2200766.

Liu, Z., Meyers, M.A., Zhang, Z. & Ritchie, R.O. (2017) Functional gradients and heterogeneities in biological materials: design principles, functions, and bioinspired applications. *Progress in Materials Science*, 88, 467–498.

Lomakin, J., Huber, P.A., Eichler, C., Arakane, Y., Kramer, K.J., Beeman, R.W. et al. (2011) Mechanical properties of the beetle elytron, a biological composite material. *Biomacromolecules*, 12, 321–335.

Montroni, D., Sparla, F., Fermani, S. & Falini, G. (2021) Influence of proteins on mechanical properties of a natural chitin-protein composite. *Acta Biomaterialia*, 120, 81–90.

Naleway, S.E., Porter, M.M., McKittrick, J. & Meyers, M.A. (2015) Structural design elements in biological materials: application to bioinspiration. *Advanced Materials*, 27, 5455–5476.

Nikolov, S., Fabritius, H., Petrov, M., Friak, M., Lymperakis, L., Sachs, C. et al. (2011) Robustness and optimal use of design principles of arthropod exoskeletons studied by ab initio-based multiscale simulations: the example of lobster cuticle. *Advanced Materials*, 22, 519–526.

Oh, J.K., Behmer, S.T., Marquess, R., Yegin, C., Scholar, E.A. & Akbulut, M. (2017) Structural, tribological, and mechanical properties of the hind leg joint of a jumping insect: using katydids to inform bioinspired lubrication systems. *Acta Biomaterialia*, 62, 284–292.

Oliver, W.C. & Pharr, G.M. (1992) An improved technique for determining hardness and elastic modulus using load and displacement sensing indentation experiments. *Journal of Materials Research*, 7, 1564–1583.

Oster, G.F. & Wilson, E.O. (1978) Caste and ecology in the social insects. *Monographs in Population Biology*, 12, 1–354.

Peisker, H., Michels, J. & Gorb, S.N. (2013) Evidence for a material gradient in the adhesive tarsal setae of the ladybird beetle *Coccinella septempunctata*. *Nature Communications*, 4, 1661.

Polidori, C. & Wurdack, M. (2019) Mg-enriched ovipositors as a possible adaptation to hard-skinned fruit oviposition in *Drosophila suzukii* and *D. Subpulchrella*. *Arthropod-Plant Interactions*, 13, 551–560.

Politi, Y., Bar-On, B. & Fabritius, H.O. (2019) Mechanics of arthropod cuticle-versatility by structural and compositional variation. In: Estrin, Y., Bréchet, Y., Dunlop, J. & Fratzl, P. (Eds.) *Architectured materials in nature and engineering. Springer series in materials science*, Vol. 282. Cham: Springer, pp. 287–327.

Politi, Y., Priewasser, M., Pippel, E., Zaslansky, P., Hartmann, J., Siegel, S. et al. (2012) A spider's fang: how to design an injection needle using chitin-based composite material. *Advanced Functional Materials*, 22, 2519–2528.

Pontin, M.G., Moses, D.N., Waite, J.H. & Zok, F.W. (2007) A nonmineralized approach to abrasion-resistant biomaterials. *Proceedings of the National Academy of Sciences of the United States of America*, 104, 13559–13564.

Püffel, F., Johnston, R. & Labonte, D. (2023) A biomechanical model for the relation between bite force and mandibular opening angle in arthropods. *Royal Society Open Science*, 10, 221066.

Püffel, F., Meyer, L., Imirzian, N., Roces, F., Johnston, R. & Labonte, D. (2023) Developmental biomechanics and age polyethism in leaf-cutter ants. *Proceedings of the Royal Society B: Biological Sciences*, 290, 20230355.

Püffel, F., Pouget, A., Liu, X., Zuber, M., van de Kamp, T., Roces, F. et al. (2021) Morphological determinants of bite force capacity in insects: a biomechanical analysis of polymorphic leaf-cutter ants. *Journal of the Royal Society Interface*, 18, 20210424.

Püffel, F., Roces, F. & Labonte, D. (2023) Strong positive allometry of bite force in leaf-cutter ants increases the range of cuttable plant tissues. *Journal of Experimental Biology*, 226, jeb245140.

Qi, H., Ma, Z., Xu, Z., Wang, S., Ma, Y., Wu, S. et al. (2023) The design and experimental validation of a biomimetic stubble-cutting device inspired by a leaf-cutting ant's mandibles. *Biomimetics*, 8, 555.

Quicke, D.L.J., Palmer-Wilson, J., Burrough, A. & Broad, J.R. (2004) Discovery of calcium enrichment in cutting teeth of parasitic wasp ovipositors (Hymenoptera: Ichneumonoidea). *African Entomology*, 12, 259–264.

Richter, A. & Economo, E.P. (2023) The feeding apparatus of ants: an overview of structure and function. *Philosophical Transactions of the Royal Society, B: Biological Sciences*, 378, 20220556.

Richter, A., Hita Garcia, F., Keller, R.A., Billen, J., Economo, E.P. & Beutel, R.G. (2020) Comparative analysis of worker head anatomy of *Formica* and *Brachyponera* (Hymenoptera: Formicidae). *Arthropod Systematics & Phylogeny*, 78, 133–170.

Schofield, R., Nesson, M., Richardson, K. & Wyeth, P. (2003) Zinc is incorporated into cuticular "tools" after ecdysis: the time course of the zinc distribution in "tools" and whole bodies of an ant and a scorpion. *Journal of Insect Physiology*, 49, 31–44.

Schofield, R.M., Nesson, M.H. & Richardson, K.A. (2002) Tooth hardness increases with zinc-content in mandibles of young adult leaf-cutter ants. *Naturwissenschaften*, 89, 579–583.

Schofield, R.M.S., Bailey, J., Coon, J.J., Devaraj, A., Garrett, R.W. & Goggans, M.S. (2021) The homogenous alternative to biomineralization: Zn- and Mn-rich materials enable sharp organismal "tools" that reduce force requirements. *Scientific Reports*, 11, 17481.

Schroeder, T.B.H., Houghtaling, J., Wilts, B.D. & Mayer, M. (2018) It's not a bug, It's a feature: functional materials in insects. *Advanced Materials*, 30, 1705322.

Smith, C.W., Herbert, R., Wootton, R.J. & Evans, K.E. (2000) The hind wing of the desert locust (*Schistocerca gregaria* Forskal). II. Mechanical properties and functioning of the membrane. *Journal of Experimental Biology*, 203, 2933–2943.

Stamm, K., Saltin, B.D. & Dirks, J.H. (2021) Biomechanics of insect cuticle: an interdisciplinary experimental challenge. *Applied Physics A*, 127, 329.

Tadayon, M., Younes-Metzler, O., Shelef, Y., Zaslansky, P., Rechels, A., Berner, A. et al. (2020) Adaptations for wear resistance and damage resilience: micromechanics of spider cuticular "tools". *Advanced Functional Materials*, 30, 2000400.

van der Wal, P., Giesen, H.J., & Videler, J.J. (1999) Radular teeth as models for the improvement of industrial cutting devices. *Materials Science and Engineering: C*, 7(2), 129–142. https://doi.org/10.1016/s0928-4931(99)00129-0

Vincent, J.F.V. (2002) Arthropod cuticle—a natural composite shell system. *Composites Part A: Applied Science and Manufacturing*, 33, 1311–1315.

Vincent, J.F.V. & Wegst, U.G.K. (2004) Design and mechanical properties of insect cuticle. *Arthropod Structure & Development*, 33, 187–199.

Waite, J.H., Lichtenegger, H.C., Stucky, G.D. & Hansma, P. (2004) Exploring molecular and mechanical gradients in structural bioscaffolds. *Biochemistry*, 43, 7653–7662.

Wang, L.-Y., Jafarpour, M., Lin, C.-P., Appel, E., Gorb, S.N. & Rajabi, H. (2019) Endocuticle sclerotisation increases the mechanical stability of cuticle. *Soft Matter*, 15, 8272–8278.

Wang, Y., Liu, C., Du, J., Huang, J., Zhang, S. & Zhang, R. (2018) The microstructure, proteomics and crystallization of the limpet teeth. *Proteomics*, 18, e1800194.

Weaver, J.C., Aizenberg, J., Fantner, G.E., Kisailus, D., Woesz, A., Allen, P. et al. (2007) Hierarchical assembly of the siliceous skeletal lattice of the hexactinellid sponge *Euplectella aspergillum*. *Journal of Structural Biology*, 158, 93–106.

Weaver, J.C., Milliron, G.W., Miserez, A., Evans-Lutterodt, K., Herrera, S., Gallana, I. et al. (2012) The stomatopod dactyl club: a formidable damage-tolerant biological hammer. *Science*, 336, 1275–1280.

Weaver, J.C., Wang, Q., Miserez, A., Tantuccio, A., Stromberg, R., Bozhilov, K.N., Maxwell, P., Nay, R., Heier, S.T., DiMasi, E., & Kisailus, D. (2010). Analysis of an ultra hard magnetic biomineral in chiton radular teeth. *Materials Today*, 13(1–2), 42–52. https://doi.org/10.1016/s1369-7021(10)70016-x

Wetterer, J.K. (1999) The ecology and evolution of worker size-distribution in leaf-cutting ants (Hymenoptera: Formicidae). *Sociobiology*, 34, 119–144.

Whitehouse, M.E.A. & Jaffe, K. (1996) Ant wars: combat strategies, territory and nest defense in the leaf-cutting ant *Atta laevigata*. *Animal Behaviour*, 51, 1207–1217.

Wilson, E.O. (1980) Caste and division of labor in leaf-cutter ants (Hymenoptera: Formicidae: *Atta*). *Behavioral Ecology and Sociobiology*, 7, 143–156.

Wilson, E.O. (1983) Caste and division of labor in leaf-cutter ants (Hymenoptera: Formicidae: *Atta*). *Behavioral Ecology and Sociobiology*, 14, 55–60.

Wilson, E.O. (1987) Causes of ecological success: the case of the ants. *Journal of Animal Ecology*, 56, 1–9.

Wirth, R., Herz, H., Ryel, R.J., Beyschlag, W. & Hölldobler, B. (2002) Herbivory of leaf-cutting ants. A case study on *Atta colombica* in the tropical rainforest of Panama. *Ecological Studies*, 164, 1–233.

Yamamoto, T., Hasegawa, T., Sasaki, M., Hongo, H., Tabata, C., Liu, Z. et al. (2012) Structure and formation of the twisted plywood pattern of collagen fibrils in rat lamellar bone. *Journal of Electron Microscopy (Tokyo)*, 61, 113–121.

Yang, W., Sherman, V.R., Gludovatz, B., Mackey, M., Zimmermann, E.A., Chang, E.H. et al. (2014) Protective role of *Arapaima gigas* fish scales: structure and mechanical behavior. *Acta Biomaterialia*, 10, 3599–3614.

Zhang, W., Xu, J. & Yu, T.X. (2022) Dynamic behaviors of bio-inspired structures: design, mechanisms, and models. *Engineering Structures*, 265, 114490.

Zhang, Y., Paris, O., Terrill, N.J. & Gupta, H.S. (2016) Uncovering three-dimensional gradients in fibrillar orientation in an impact-resistant biological armour. *Scientific Reports*, 6, 26249.

Zhang, Z., Zhang, Y., Zhang, J. & Zhu, Y. (2019) Structure, mechanics and material properties of claw cuticle from mole cricket *Gryllotalpa orientalis*. *PLoS One*, 14, e0222116.

Zimmermann, E., Gludovatz, B., Schaible, E., Dave, N.K.N., Yang, W., Meyers, M.A. et al. (2013) Mechanical adaptability of the Bouligand-type structure in natural dermal armour. *Nature Communications*, 4, 2634.

SUPPORTING INFORMATION

Additional supporting information can be found online in the Supporting Information section at the end of this article.

Table S1. Quantity of measurements by nanoindentation for each individual ant, cuticle layer, region, and testing direction.

Table S2. Quantity of measurements by elemental analysis for each individual ant, cuticle layer, region, and testing direction.

Table S3. For the mediae and minims along the circumferential axis—mean and standard deviation values of the elemental composition, given in atomic %.

Table S4. For the mediae—results from pairwise comparison for each element.

Table S5. For the minims—results from pairwise comparison for each element.

Table S6. For the mediae and minims—mean and standard deviation of the mechanical parameters *H* and *E*, both given in GPa. *N*, quantity of tested regions; SD, standard deviation.

Table S7. For *E* and *H* of mediae and minims—results from pairwise comparison between the cuticle layers.

Table S8. For *E* and *H* of mediae and minims—results from pairwise comparison for the regions of interest.

Table S9. For the mediae and minims—results from pairwise comparison for the regions of interest.

Figure S1. Elemental composition for the exo-, meso-, and endocuticle of the minims and mediae, given in atomic %.

Figure S2. Young's modulus *E* values, given in GPa, for each cuticle layer of the two castes, tested in circumferential and longitudinal direction.

Figure S3. Relationship between hardness (in GPa) and Ca (in atomic %) with standard deviation bars for all mandibles and all tested regions.

Figure S4. Relationship between Young's modulus (in GPa) and Ca (in atomic %) with standard deviation bars for all mandibles and all tested regions.

Figure S5. Relationship between hardness (in GPa) and Cl (in atomic %) with standard deviation bars for all mandibles and all tested regions.

Figure S6. Relationship between Young's modulus (in GPa) and Cl (in atomic %) with standard deviation bars for all mandibles and all tested regions.

Figure S7. Relationship between hardness (in GPa) and Cu (in atomic %) with standard deviation bars for all mandibles and all tested regions.

Figure S8. Relationship between Young's modulus (in GPa) and Cu (in atomic %) with standard deviation bars for all mandibles and all tested regions.

Figure S9. Relationship between hardness (in GPa) and Fe (in atomic %) with standard deviation bars for all mandibles and all tested regions.

Figure S10. Relationship between Young's modulus (in GPa) and Fe (in atomic %) with standard deviation bars for all mandibles and all tested regions.

Figure S11. Relationship between hardness (in GPa) and Mg (in atomic %) with standard deviation bars for all mandibles and all tested regions.

Figure S12. Relationship between Young's modulus (in GPa) and Mg (in atomic %) with standard deviation bars for all mandibles and all tested regions.

Figure S13. Relationship between hardness (in GPa) and Mn (in atomic %) with standard deviation bars for all mandibles and all tested regions.

Figure S14. Relationship between Young's modulus (in GPa) and Mn (in atomic %) with standard deviation bars for all mandibles and all tested regions.

Figure S15. Relationship between hardness (in GPa) and Si (in atomic %) with standard deviation bars for all mandibles and all tested regions.

Figure S16. Relationship between Young's modulus (in GPa) and Si (in atomic %) with standard deviation bars for all mandibles and all tested regions.

Figure S17. Relationship between hardness (in GPa) and Zn (in atomic %) with standard deviation bars for all mandibles and all tested regions.

Figure S18. Relationship between Young's modulus (in GPa) and Zn (in atomic %) with standard deviation bars for all mandibles and all tested regions.

How to cite this article: Krings, W., Birkenfeld, V. & Gorb, S.N. (2025) Mechanical properties and cuticle organisation in mandibles are related to the task specialisation in leafcutter ants (*Atta laevigata*, Attini, Formicidae). *Physiological Entomology*, 50(2), 152–165. Available from: https://doi.org/10.1111/phen.12476